Nematic textures in colloidal dispersions of Na-fluorohectorite synthetic clay

N. I. Ringdal, D. M. Fonseca, E. L. Hansen,* H. Hemmen, and J. O. Fossum†
Department of Physics, Norwegian University of Science and Technology, Hoegskoleringen 5, N-7491 Trondheim, Norway
(Received 18 November 2009; published 7 April 2010)

We have studied stable strata of gravity-induced phase separation in suspensions of synthetic Na-fluorohectorite clay in saline solutions. We have observed how the strata depend on clay concentration as well as on salt content. The mass distribution and density variation at the isotropic-nematic interface indicate that existing models and assumptions in existing simulations are able to relatively well account for the observed behavior. We suggest that discrepancies could be due to the high polydispersity and the irregular shape of our Na-fluorohectorite particles, as well as diffusive double-layer effects, which could result in a competition between nematic ordering and gelation. The dependence on ionic strength displays three main regimes irrespective of clay concentration. At low ionic strength ($\approx 0.1-5$ mM NaCl), the Debye screening length is longer than the van der Waals force range. In this regime, the particles repel each other electrostatically and entropy-driven Onsager-type nematic ordering may occur, although gelation effects could also play a role. For ionic strengths above about 5 mM, we believe that the van der Waals force comes into play and that particles attract each other locally according to the classical Derjaguin, Landau, Verwey, and Overbeek (DLVO) model of colloid interactions, resulting in a small-domain regime of attractive nematiclike ordering. In the third regime, for ionic strengths above ≈ 10 mM, the clay particles aggregate into larger assemblies, due to the dominant van der Waals force, and the observed birefringency is reduced. We have studied the nematic phase in detail between crossed polarizers and have found textures showing nematic Schlieren patterns. By rotating the polarizers as well as the samples, we have observed examples of disclinations of strengths -1, $-1/2$, and $+1$.

DOI: 10.1103/PhysRevE.81.041702 PACS number(s): 61.30.Eb, 61.30.Jf, 61.30.Gd, 64.75.Xc

I. INTRODUCTION

The formation of liquid-crystalline order in colloidal dispersions of anisotropic mineral nanoparticles has recently seen an increased research activity [1–3]. From early investigations of colloidal systems such as vanadium pentoxide (V_2O_5) [4] and tobacco mosaic virus [5,6], suspensions of various rodlike nanoparticles [7] have been found to exhibit a spontaneous transition from an isotropic (*I*) to a nematic (*N*) phase, in good agreement with statistical mechanical theories. In the 1940s, Onsager [8] modeled this phase transition considering the competition between the entropy of orientation (favoring orientational randomness) and the entropy of excluded volume (favoring nematic alignment) of the colloidal system, thus concluding that at a sufficiently high particle concentration, the packing (excluded volume) entropy dominates and it becomes favorable for the particles to order in nematic alignment. Onsager showed that interparticle interactions beyond hard-core repulsion are not necessary for orientational ordering and that the shape anisotropy of the particles alone is enough to drive the *I*-*N* phase transition. As Onsager proposed and as was later confirmed by computer simulations [9,10], nematic ordering occurs for platelike particles that are fairly anisometric. This possibility had already been studied experimentally by Langmuir in 1938 [11], who reported observations of an *I*-*N* phase transition in sols of natural clay particles, although conclusive evidence for a true thermodynamically stable *I*-*N* transition was lacking.

An obstacle encountered when using clays as models to study nematic ordering of colloidal systems is the tendency for clays to gel when dispersed in water. This transition from a sol to a gel may take place at very low clay concentrations. The gel structure and its formation, which are responsible for many of the practical applications of clays, have been substantially studied from the 1930 to 1950s [12–16] and until today [17–35]. In recent years, the presence of orientational order in clay gels have been documented by optical measurements [30,36] showing visual nematic textures. Neutron- [37–39] and x-ray-scattering [40–43] as well as magnetic-resonance imaging (MRI) experiments [44–49] have all revealed structural correlations with nematic order in clay gels. However, since the gel phase may not be at thermodynamic equilibrium, the nematic ordering in the gels cannot be explained by Onsager theory alone.

There is today no complete theory for the process of orientational ordering in a gelled clay structure. There has been suggestions that the sol-gel transition may be directly related to the *I*-*N* transition [29,30,50,51], but this possibility has been contradicted in experiments by Michot *et al.* [27], showing that the concentration for the sol-gel transition of suspensions of size-selected Wyoming Na-montmorillonite increases linearly with particle anisotropy. This is opposite to what could be expected for the corresponding evolution of the *I*-*N* transition, since a large aspect ratio for the particles shifts the *I*-*N* transition toward lower volume fractions. Other studies concerning systems of charged colloidal platelets, such as Mg_2Al layered double hydroxide [52] and gibbsite [53,54], also suggest that the liquid crystal phase transition and gelation are separate and possibly competitive processes. In these latter two systems, the *I*-*N* phase transition has been observed to take place at a lower concentration

*elisabeth.hansen@ntnu.no
†jon.fossum@ntnu.no

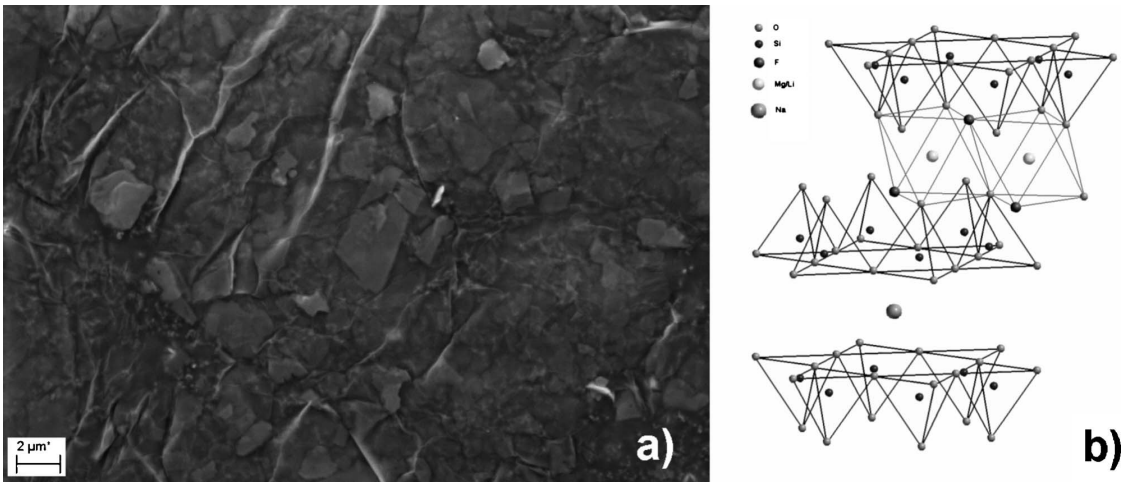

FIG. 1. (a) SEM micrograph of NaFh particles and (b) the idealized crystalline structure of one Na-fluorohectorite layer. The NaFh particles in the SEM image consist of several such crystalline layers of approximately 1 nm thickness that are stacked in a lamellar structure through the sharing of intercalated Na^+ ions between the layers.

than the sol-gel transition [52,55,56]. Thermodynamic stability of the nematic ordering could therefore be achieved and be further compared to the Onsager model. For clay platelets, an *I-N* transition was recently obtained in suspensions of natural nontronite [57,58]. Experimental systems of colloidal clay suspensions should be expected to differ from the Onsager model, since factors such as particle morphology, electrostatic and van der Waals forces [59], the gravitational force [60–62], and Brownian motion [63,64] are of importance to the phase behavior.

In the present paper, we describe the phase behavior of the synthetic 2:1 phyllosilicate smectite clay Na-fluorohectorite (NaFh) suspended in aqueous solutions with NaCl concentrations ranging over more than 2 orders of magnitude from 0.1 to 25 mM. In the gravitational field, a suspension of NaFh may be effectively separated into different strata of gels, sols, and sediments. In one of the phases, collective particle orientation corresponding to nematic order is found as evidenced by previous x-ray scattering [27,41,65–67] and MRI [44] studies.

Here, we present the birefringent nature of the nematic ordering, the role of different salt concentrations, and study how the clay concentration varies in the gravity-dispersed suspensions. We also report on observations of topological defects in the nematic phase. It is known that many of the topological defects which are commonly present in molecular liquid crystals may also form in mineral liquid crystals. Schlieren textures and different disclinations have been observed in nematic clay gels of bentonite and Laponite [36] and in the nematic phase of other systems of nanoplatelets [55,68] similar to our present observations.

II. EXPERIMENTAL DETAILS

A. Materials

Synthetic Li-fluorohectorite clay was purchased in powder form from Corning Inc., New York, and later ion-exchanged to produce Na-fluorohectorite. The nominal chemical formula for NaFh is $Na_{0.6}Mg_{2.4}Li_{0.6}Si_4O_{10}F_2$, for which two inverted silicate tetrahedral layers share their apical oxygens with one octahedral layer (Fig. 1). The individual NaFh particles are composed of such silicate lamellae [69] that stack by sharing Na^+ ions between their basal planes. Each 2:1 silicate lamellae is around 1-nm thick, with a nominal charge of 1.2 e^- per unit cell (Si_8O_{20}) due to substitutions of Li for Mg in the octahedral layers. This nominal layer charge is relatively large compared to that of other smectite clays, such as synthetic Laponite RD (0.4 e^-/unit cell) and natural montmorillonite (0.6 e^-/unit cell) [69]. The large layer charge is responsible for the particle stacks remaining intact when suspended in water, in contrast to what is the case for Laponite RD and montmorillonite [40]. Scanning electron microscopy (SEM) images (Fig. 1) indicate that the polydispersity in NaFh particle sizes is quite large and that it is accompanied by highly variable particle morphologies. The effective diameter of the platelets can vary from a few hundred nanometers up to about 20 μm [69].

The ion-exchange process consisted of adding 70 g of the purchased Li-intercalated fluorohectorite to 1000 ml distilled and de-ionized water, where it was dissolved and stirred by shaking for 2 days using an incubator at 300 rpm. Sodium ions were added as 60 g NaCl, which corresponds to about 10 times the known layer charge per unit cell. The suspension was further shaken at 300 rpm for 2 weeks. Cl^- ions were removed by dialysis, where the Cl^- content was checked regularly using a standard silver nitrate procedure. NaFh powder was obtained by drying the resultant solution at 105 °C for about 3 days. A mortar and pestle was used before the NaFh powder was further pulverized using a milling machine (IKA A11 basic).

Three different batches of NaFh were studied in the present experiments and are referred to as B1, B2, and B3, respectively. All three batches were prepared as described above. Due to some differences in the time sequences spent at the different preparation steps and due to differences in crushing and milling procedures, there may be differences between the particle sizes of the three batches, so that the

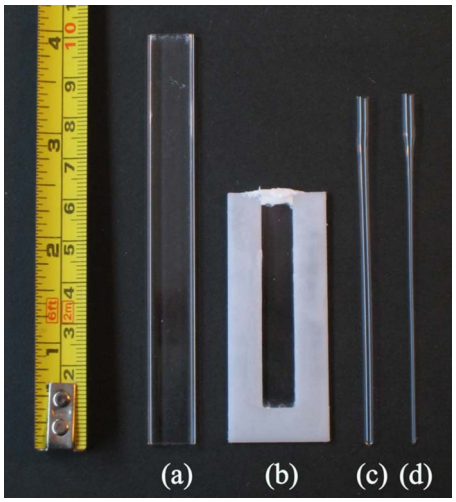

FIG. 2. (Color online) Different sample tubes used in the experiments: (a) Vitrotube 4410-100 from VitroCom; (b) rectangular cell made from POM plastic and microscope glass covers; [(c) and (d)] Hilgenberg Mark tubes of diameters 2 mm (left) and 1 mm (right).

particles of batch B1 and B2 are similar, whereas the B3 particles are expected to be smaller.

B. Experimental methods

Dispersions of the B1, B2, and B3 batches of NaFh in saline solutions were prepared with varying clay and salt concentrations and allowed to settle under the influence of gravity for several weeks in containers suited either for birefringence imaging or x-ray studies, or in larger containers. Birefringence images were recorded with the samples placed between crossed polarizers and illuminated with a diffusive white light source and images were captured with a charge coupled device (CCD) camera. The x-ray scattering studies were conducted in part at an in-house Bruker system and in part at the Dutch-Belgian beamline (DUBBLE) at the European Synchrotron Radiation Facility (ESRF). The Bruker system used an x-ray wavelength of 1.54 Å with an accessible q range of approximately 0.3–4 nm^{-1} and a two-dimensional (2D) multiwire gas detector for data acquisition. The setup at DUBBLE had an x-ray wavelength of 1.03 Å and an accessible q range of approximately 0.06–0.6 nm^{-1}, with a 2D multiwire gas detector.

Two kinds of rectangular sample tubes were used for optical studies of the phase behavior of the suspensions. Figure 2(a) shows a Vitrotube 4410–100 from VitroCom, which is 10-cm long, 1-cm wide, and 1-mm thick. Figure 2(b) shows a cell made of polyoxymethylene (POM) plastic with microscope cover glass as windows, with inner dimensions of 2460×1 mm^3. This cell has glass walls approximately 0.12-mm thick. Figures 2(c) and 2(d) display the cylindrically shaped thin-walled capillary tubes used in some of the optical studies and for the x-ray scattering; these are 2 and 1 mm Hilgenberg Mark tubes.

III. RESULTS

A. Clay concentration

Shown in Fig. 3 are birefringence images of seven B1 samples with NaFh concentrations of 0.5, 1, 2, 3, 4, 5, and

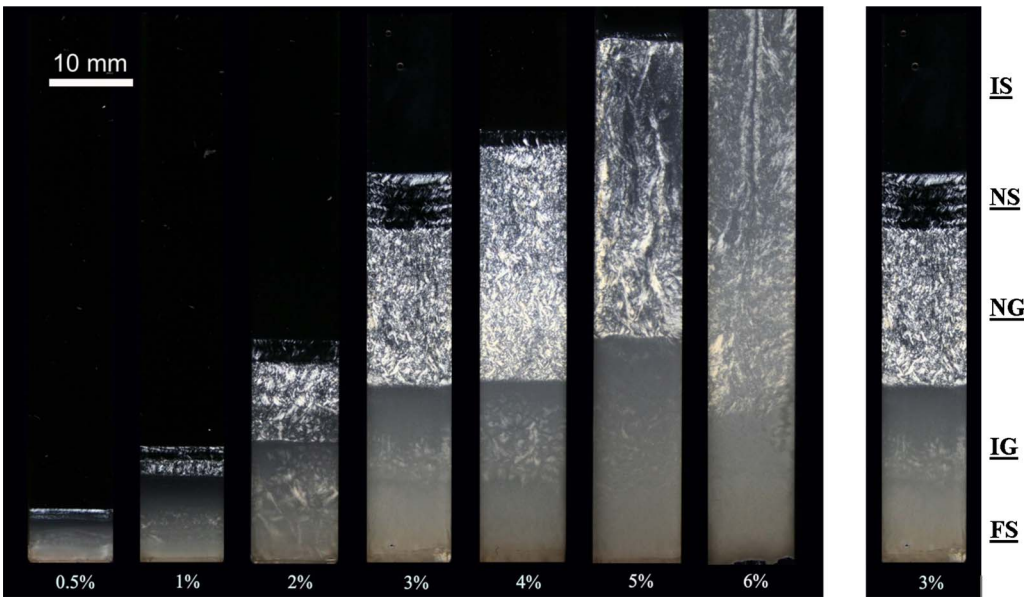

FIG. 3. (Color online) Samples of suspended B1 batch Na-fluorohectorite particles at concentrations of 0.5, 1, 2, 3, 4, 5, and 6 wt % clay in 1 mM NaCl solutions in water. The photographs were taken at different times after the samples had started to settle under gravity; these times were 1 month for the 0.5% by weight sample, 2.5 months for 1%, 3 months for 3% and 5%, 4 months for 6%, and 4.5 months for 2% and 4%. The picture of the 3% sample represents the stabilized settling state, where no further changes in the phases are observed; for the other samples, a moderate increase in the extent of the NS phase along with a slight increase in overall birefringence is expected as the samples age. The 3% sample is expected to look the same after 4.5 months and can be directly compared to the 2% and 4% samples. As shown, the 3 wt % sample displays IS, NS, NG, (mainly) IG, and FS.

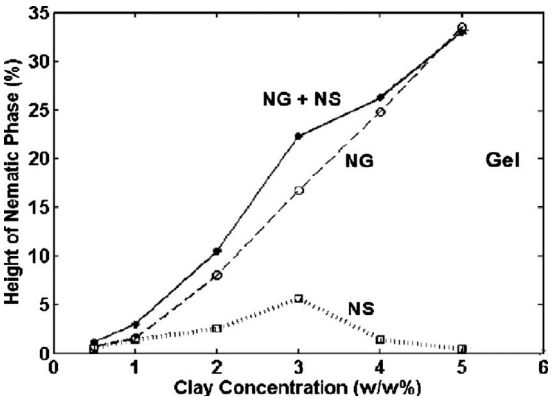

FIG. 4. Fraction of the total sample height occupied by the nematic phases for the B1 powder at ionic strength 1 mM NaCl for clay concentrations in the range of from 0.5 to 5 wt %. The total height of the sample is almost 10 cm; hence the indicated height percentage is numerically equal to the height of the nematic phase in millimeters. Here, NG and NS denote nematic gel and nematic sol, respectively.

6% by weight of clay at 1 mM NaCl. The behavior of the samples depicted in Fig. 3 is typical for our system. The samples in the concentration range from 0.5% to 5% by weight of clay display (from bottom to top) a flocculated sediment (FS), followed by a gel-like sediment (IG) that is mainly isotropic, but with modestly birefringent domains, a nematic phase that may be split into a lower, gelled phase (NG) and an upper nematic sol (NS) phase, and finally an isotropic sol (IS). The designation of the various phases as being gels or sols refers to qualitative observations and will in later works be further investigated by rheological studies. The time scale for the formation of the different phases varies. In particular, the formation of the nematic sol happens in general on a much slower time scale (weeks) than the formation of the nematic gel (days).

The main differences between the three batch powders are variations in the location of phase boundaries and hence in the relative fraction of sample volumes occupied by the phases. For the samples with the lowest clay concentrations, the relative amount of birefringence is in general lower for the same induced phase than for samples of higher concentration.

The contribution of the sediment and the isotropic gel above it to the sample height increases as expected when the clay concentration is increased, up to the point of 6 wt %, where the behavior changes. For the 0.5%–5% samples, a density profile is observed which includes the FS, IG, NG, NS, and IS phases. This is common to all of the samples in the 0.5%–5% concentration range.

For the 2 wt % B1 sample, the birefringent NG part of the sample can be divided into two regions with an upper part being more birefringent than the lower. At 6 wt %, the distinction between the phases is less obvious than in the other samples, although some birefringence is observed for this sample as well. The relative heights for the nematic phase of the samples shown in the Fig. 3 were measured and are plotted in Fig. 4.

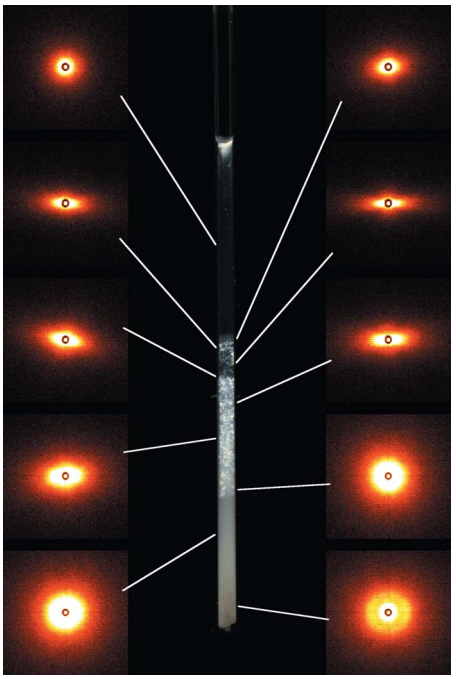

FIG. 5. (Color online) Example of a sample prepared in a 2 mm capillary tube and the corresponding SAXS patterns recorded at different heights in the tube showing anisotropies as previously observed by us in other NaFh samples [41,65–67]. We see that in the nematic part of the samples, the long axis of the SAXS pattern is horizontal, indicating that the platelet normals also are horizontal. The greatest anisotropy is found in the NS region.

Figure 5 shows an example of a sample prepared in a capillary tube and the corresponding small-angle x-ray scattering (SAXS) patterns recorded at different heights in the tube, showing anisotropies as previously observed by us in other NaFh samples [41,65–67]. The SAXS data were obtained on the in-house commercial Bruker SAXS instrument. We see that in the nematic part of the samples, the long axis of the SAXS pattern is horizontal, indicating that the platelet normals and hence the nematic director also are horizontal [66,67].

B. Mass distribution

In order to map out density differences between the various phases and how much the density varies within each phase, the clay contents were measured for two samples of 3 wt % NaFh (B2 and B3 samples) at 1 mM NaCl. These samples were prepared in containers of 50 ml each, all with height 7.5 cm and diameter 2.9 cm. The samples were left to settle for 2 months (B2) and 2.5 months (B3) before the measurements, and after this waiting time, phase separation into the previously described static strata had occurred.

The clay content measurements were carried out by pipetting out 250 μl at a time by inserting a pipette at the top of the sample. The measurements extended from the isotropic liquid at the top to the sediment at the bottom. In total, 177 measurements were done for the B3 sample and 163 for the B2 sample. Since it turned out to be difficult to pipette out the strongly gelled bottom phase and sediment, the remain-

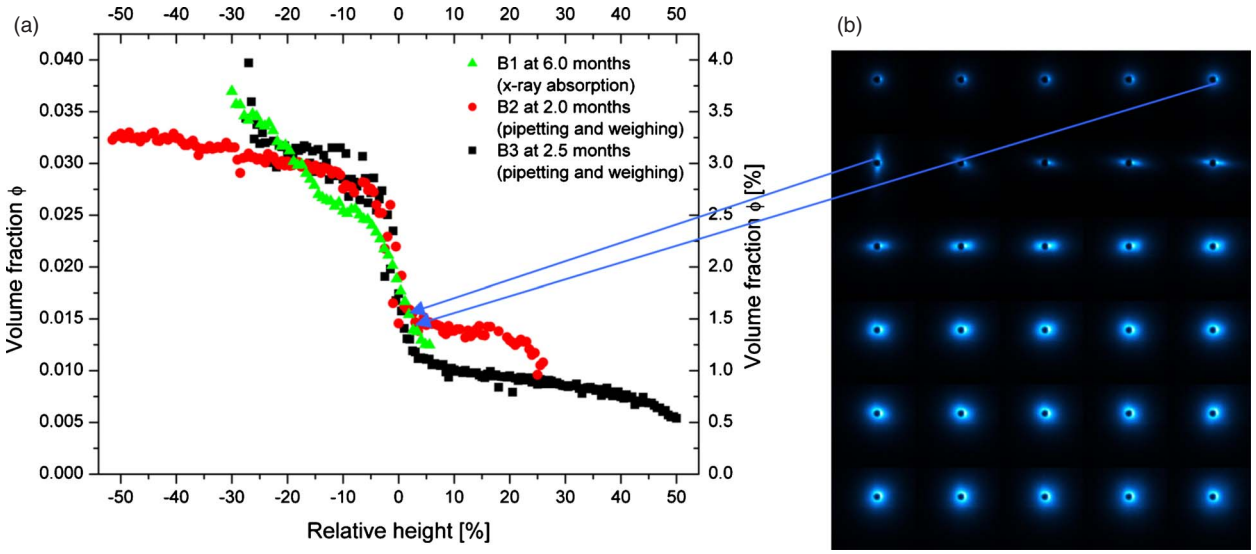

FIG. 6. (Color online) (a) Clay concentration as function of relative sample height for initially 3 wt % samples at 1 mM NaCl: B1 sample (green triangles), B2 sample (red circles), and B3 sample (black squares). The relative height gives the height at which a measurement was taken in percentage relative to the full height of the sample dispersion. The zero reference point has been shifted from the bottom of the capillary to the gap between the nematic and isotropic phases for clarity. The B2 and B3 data series were determined by pipetting out successive 250 μl batches and weighing them, whereas the B1 series was obtained from x-ray absorption data recorded at the DUBBLE beamline at ESRF. (b) Montage of the raw SAXS data (height in sample decreasing by 1 mm from top left to bottom right) shows that the B1 system actually transitions from an isotropic to an ordered state between two data points.

ing phases at the bottom of each sample were dried and weighed to contain 0.285 g of NaFh for the B3 sample (8.5 mm) and 0.561 g for the B2 sample (14 mm).

Figure 6 shows the clay volume fraction as a function of relative height. The relative height is the height where a sample was extracted, represented as a percentage of the full sample height. The zero reference point is set to the gap between the nematic regions and the isotropic sol phase. The volume fraction was found by evaluating the excess weight of each pipetted 250 μl batch using a value of 2.0 g/cm^3 for the mass density of NaFh particles intercalating two water layers [70]. Figure 6 also shows the volume fraction of clay as a function of relative height in a capillary sample of B1 batch NaFh. This series was calculated from x-ray absorption data obtained at the DUBBLE beamline at ESRF at a wavelength of 1.03 Å. The absorption coefficients of clay, water, and salt were computed at the relevant wavelength and the sample thickness was set to a value of 1.22 mm, which is within the accuracy of the Mark tube nominal diameter value of 1 mm. Figure 6 also illustrates how the marked step in concentration shown in the three graphs does not reflect the gap in volume fraction between the isotropic and nematic phases. The transition from the isotropic to the ordered state for the B1 system is, through the anisotropy of

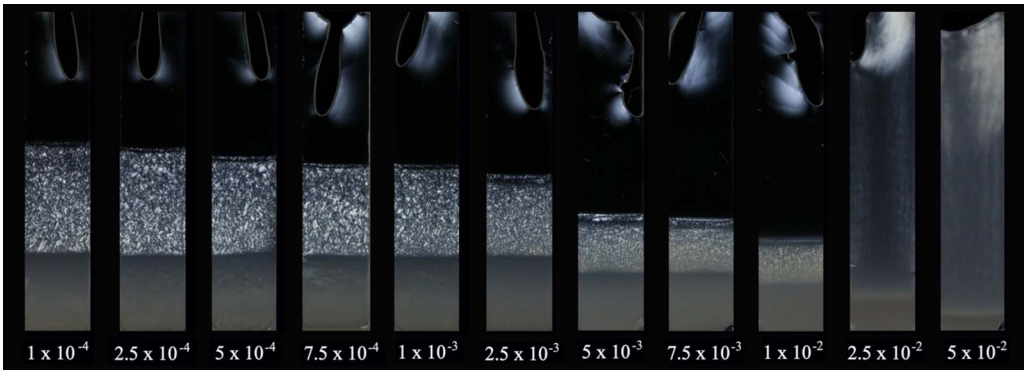

FIG. 7. (Color online) Birefringence images of 3 wt % B1 samples at NaCl concentrations ranging from 0.1 to 50 mM. The samples were prepared in POM cells [shown in Fig. 2(b)] and the birefringent structures at the top parts are due to local increases in clay concentration caused by water evaporation. The pictures were taken with the samples placed between crossed polarizers with their transmission axes oriented parallel and perpendicular with the long axis of the containers. The relative height of the nematic phase decreases with ionic strength as the electrostatic interaction is more effectively screened, thus reducing the effective clay volume fraction of the dispersions. The postulated transition between phase behaviors dominated by repulsive and attractive forces happens at an ionic strength between 10 and 25 mM.

the SAXS patterns recorded along with the transmission data, shown to occur between calculated volume fractions of, respectively, 1.39% and 1.54%.

C. Salt concentration

Salt concentration is known to play a major role in the phase behavior of aqueous Na-fluorohectorite solutions owing to particle surface charges [40,41]. Figure 7 shows a series of 3 wt % B1 samples with an increasing salt concentration ranging from 0.1 to 50 mM NaCl. Although only B1 samples are shown, all sample batches show the same general trend as that found in Fig. 7, irrespective of powder type and clay concentration. At low salt concentrations, the phase separation exhibits the formation of a nematic phase between a flocculated gel at the bottom and an upper dilute isotropic sol. As the samples age beyond the time span required for the stabilization of phase boundaries, the upper isotropic sol seems to transform into a gelled state, as illustrated by the features in the upper parts of the samples of Fig. 7. These features also display slight birefringence due to local concentration increases produced by a moderate degree of water evaporation from the sample. This very slow evaporation had no apparent effect on the birefringent textures of the NS and NG regions.

As the ionic strength is increased, the relative height of nematic phase decreases along with an increase of the upper, initially isotropic sol. In general, the relative height of the flocculated gel also moderately decreases as the ionic strength is changed from 0.1 to 1 mM NaCl. For the B1 samples in Fig. 7, this is not as pronounced as for other batches and only a slight decrease can be seen over the given range of salt concentrations. As the ionic strength is further increased, the height of the isotropic gel and the nematic phase suddenly displays a larger drop when the salt concentration is increased from 2.5 to 5 mM NaCl. Above 10 mM NaCl, there seems to be a gravity-settled equilibrium distribution of particles in the whole container.

IV. DISCUSSION

A. Discussion of mass distribution

There are small discrepancies between the B1, B2, and B3 suspensions investigated in Sec. III B regarding the clay concentration step occurring around the nematic-isotropic interface. The clay volume fractions for the B1 sample are of about 2.5% well into the nematic phase and 1.2% in the isotropic phase. For the B2 sample, these values are about 3.2% for the nematic phase and 1.4% for the isotropic phase, and for the B3 sample about 2.9% and 0.9%. Thus, the marked steps in volume fraction upon going from the isotropic state through the nematic sol state and finally into the nematic gel are of 1.3%, 1.8%, and 2.0% for the B1, B2, and B3 samples, respectively. Note, however, that from the x-ray absorption data, the actual difference in volume fraction observed at the phase interface between the isotropic and nematic (sols) is as small as 0.15%. The more marked step in volume fraction of around 1.3%–2.0% thus mainly reflects a concentration increase occurring after the threshold for nematic ordering has been crossed. The difference in volume fraction between the batches in the isotropic phase may possibly be explained by the fact that the B3 batch has been more finely crushed and therefore might have lower polydispersity and smaller particle sizes, allowing a larger fraction of the clay particles to remain dispersed in the isotropic sol phase over time.

Because of sedimentation and gelation, it is not possible to obtain samples of NaFh where isotropic or nematic phases constitute the whole volume of the sample. Figure 4 shows that the relative amount of the nematic gel increases linearly upon increasing the clay content from 1 to 5 wt % and then the isotropic gel and nematic merge into a single phase at about 6 wt %. Such a linear increase is similar to what has been observed for other systems reported in the literature, such as gibbsite [55] and nontronite [57,58], when the volume fraction was gradually increased in those systems. The gibbsite and nontronite systems have been reported to display a true thermodynamic isotropic-nematic phase transition, where attractive forces are believed not to interfere with the nematic ordering.

For gibbsite and nontronite, experimental values for the densities of the coexisting isotropic and nematic phases are in reasonable agreement with theoretical computer simulations [71] (for infinitely thin platelets) for which dimensionless number densities, i.e., the number density $n=N/V$, expressed as the number of particles N per volume unit V, multiplied by the cubed diameter D, at zero polydispersity are found to be $n_{\mathrm{iso}}D^3 \approx 3.7$ and $n_{\mathrm{nem}}D^3 \approx 4.0$. These simulations [71] were done for infinitely thin platelets, but it has also been found that platelets with a finite thickness do not give any major difference: $n_{\mathrm{iso}}D^3 \approx 3.8$ and $n_{\mathrm{nem}}D^3 \approx 3.9$ when the diameter-to-thickness ratio is 10 [10]. If the polydispersity is 25%, which would likely be a low estimate for our system, the densities are found to be $n_{\mathrm{iso}}D^3 \approx 3.5$ and $n_{\mathrm{nem}}D^3 \approx 5.0$, respectively [71].

Since the sedimentation process in our NaFh suspensions may fractionate the particles, the size (or shape) of the particles in the isotropic phase may be different from the particles in the nematic phase. This hypothesis is supported by the fact that the nematic sol forms after the nematic gel region has stabilized, something which indicates that the particles forming the nematic sol are able to stay dispersed on a longer time scale than the particles which form the nematic gel. With the possible variation of particle sizes and shapes in mind, the values reported in Fig. 6 for the volume fractions at the isotropic and nematic phases might still be used to estimate number densities, which can be compared to theoretical and other experimental [54,56] results. The relation between volume fraction ϕ and number density nD^3 for circular platelets of diameter D and thickness t is [56]

$$\phi = n\pi D^2 t/4 = (\pi/4)(t/D)(nD^3). \tag{1}$$

When polydispersity is taken into account, Eq. (1) is replaced by [56]

$$\phi = (\pi/4)(\langle t\rangle/\langle D\rangle)(n\langle D^3\rangle)(1+\sigma_D^2)/(1+3\sigma_D^2), \tag{2}$$

where $\sigma_D=[(\langle D^2\rangle-\langle D\rangle^2)^{1/2}]/\langle D\rangle$ represents the polydispersity in the diameter and $\langle\rangle$ denotes the system average [56]. Rewriting Eq. (2) gives

$$n\langle D^3\rangle = \phi(4/\pi)(\langle D\rangle/\langle t\rangle)(1+3\sigma_D^2)/(1+\sigma_D^2). \quad (3)$$

An exact value for the polydispersity of our suspensions of Na-fluorohectorite is not known, but AFM [67] and SEM pictures (Fig. 1) indicate that the polydispersity is high. In order to estimate quantities, the use of an approximated average particle diameter of 3(2) μm, which corresponds to a circle of same facial area, gives the coexisting densities of $n_{\mathrm{iso}}D^3 \approx 3.2(2.1)$ and $n_{\mathrm{nem}}D^3 \approx 3.5(2.4)$ when the effects of a high polydispersity are assumed to force the factor $(1+3\sigma_D^2)/(1+\sigma_D^2)$ to its limiting value of 3, and 50 nm is used for the average particle thickness. Previous investigations have shown however that the thickness of the particles in the isotropic phase is less than in the nematic [67] and there are also strong indications that average particle diameters could be smaller in the isotropic phase, since these particles are seen to remain dispersed on time scales of several months. Setting the average particle diameter and thickness, respectively, in the nematic phase to 4 (3) μm and 50 nm while using values of 2 (1) μm and 40 nm for the isotropic phase leads to coexisting densities of $n_{\mathrm{iso}}D^3 \approx 2.7$ (1.3) and $n_{\mathrm{nem}}D^3 \approx 4.7$ (3.5). The values are roughly comparable to the theoretical values found for polydisperse systems [71], but are also very sensitive to the unknown average particle diameter and the polydispersity in this parameter.

Computer simulations by Bates [72] showed that the coexisting densities for the nematic-isotropic transition are dependent on the shape of the particles. Bates's study showed that the transition densities for triangular particles are lower than for particles of circular shape ($n_{\mathrm{iso}}D^3 \approx 2.9$ and $n_{\mathrm{nem}}D^3 \approx 3.2$ for triangular particles; $n_{\mathrm{iso}}D^3 \approx 3.7$ and $n_{\mathrm{nem}}D^3 \approx 4.0$ for circular particles). The simulation data [72] also showed that rectangular particles with an aspect ratio of 2:1, which might be more representative of the present NaFh particles, have transition densities intermediate between the values obtained for the triangular and circular particles.

The fact that different NaFh particles within our system may interact, separate, and behave differently from each other depending on particle size could also influence the transition densities. Larger particles (2–10 μm) may form nematic ordering in coexistence with an isotropic embedding of smaller particles (<2 μm), as was also found to occur in the simulation data [71].

B. Discussion of salt concentration effects

Since a theoretical understanding of the ionic-strength-dependent ordering of charged colloidal particles of large particle size is not yet fully established, the phase behavior present in this section is qualitatively discussed within the classical Derjaguin, Landau, Verwey, and Overbeek (DLVO) [59] and Onsager theories [8]. When the samples in Fig. 7 are viewed without polarizers (not depicted), there seems to be a density increase in the lower phases as the ionic strength increases, which is expected due to the decrease in repulsion. For any clay concentration or powder type, the NaFh suspensions form loose, suspended flocs at a salt concentration of about 50 mM, and for higher ionic strengths, the flocs are denser and sediment out.

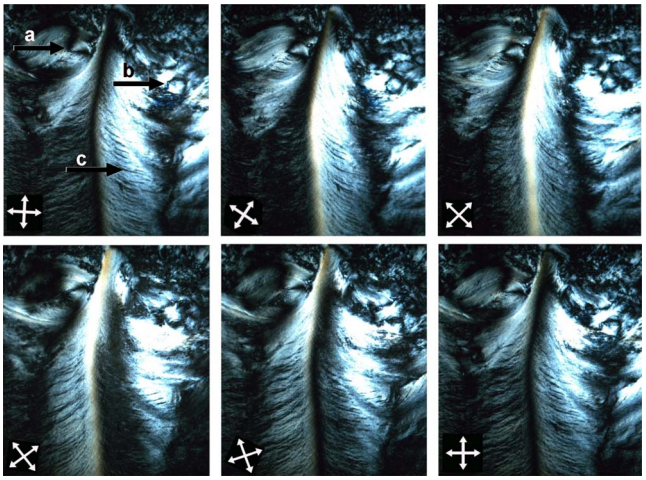

FIG. 8. (Color online) Birefringence images of a sample of 3 wt % B3 NaFh in 1 mM aqueous NaCl solution at different angles of the crossed polarizers. From the upper left to the lower right picture, the polarizers are rotated successively to 20°, 45°, 55°, 75°, and 90° with respect to the edges of the sample tube. Arrow a shows a disclination with two brushes emanating from each other at 90°. In the first two pictures of the last row, two more brushes may be seen. The brushes rotate in the same direction as the polarizers and the strength can therefore be regarded as being +1. Arrow b shows a singularity where two dark brushes meet and rotate in the opposite direction with respect to the rotation of the crossed polarizers. This corresponds to a disclination with strength −1/2. Arrow c marks the position of dark grooves located between birefringent stripes. As the polarizers are rotated, there are no apparent movements of the grooves.

In Fig. 7, a flocculation transition is found to take place between ionic strengths of 10 and 25 mM NaCl. Such a flocculation transition is similar to data found for Wyoming montmorillonite [73], where the transition line shows a negative slope as the clay concentration is increased. This is also probably the case for our NaFh system, since slightly slower coagulation occurs for the lowest clay concentration. Experiments carried out by Michot *et al.* [58] on sodium-nontronite also show a flocculation transition at ionic strength 10 mM. However, the phase diagram of this clay type has a positive flocculation slope at low volume fractions, thereafter displaying a negative sol-gel transition as the volume fraction is further increased. Compared to other clay minerals, the flocculation transition for NaFh is lower than for bentonite and higher than for Laponite [36]. Within the framework of the classical DLVO theory, a transition from a repulsive interparticle potential characterized by a high barrier toward flocculation to a potential which exhibits a minimum for a given particle separation is expected as the salt concentration is increased [59]. For our system, the sudden drop in the extent of the nematic phase between salt concentrations of 2.5 and 5 mM could indicate the introduction of effects related to attractive particle interactions, as was also concluded in [66]. The increased extent of the nematic phase for low salt concentrations as observed in Fig. 7 might indicate that the number density of particles at the isotropic-nematic transition increases as the salt concentration is increased from 0.1 to 10 mM.

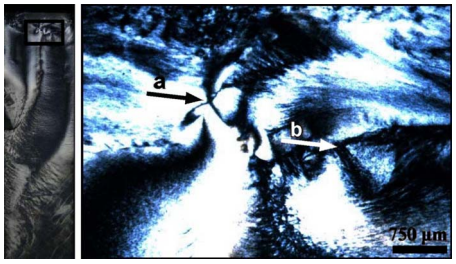

FIG. 9. (Color online) Defects in the nematic region close to the isotropic phase for a sample of 3 wt % B3 powder at 1 mM NaCl. The pictures were taken after 8 months of gravitational settling. Arrow a shows a disclination of strength −1 and arrow b shows a disclination of strength +1.

C. Discussion of Schlieren patterns, textures, and defects

Defects commonly found in thermotropic molecular liquid crystals may also be observed in colloidal systems that display orientational ordering. In Fig. 8, we show birefringence images from a sample of 3 wt% B3 NaFh in 1 mM aqueous NaCl solution at different angles of the crossed polarizers, including a disclination defect [74] with two brushes emanating from each other at 90°. In the first two pictures of the last row, two more brushes may be seen. The brushes rotate in the same direction as the polarizers and the strength is therefore +1. Arrow b shows a singularity where two dark brushes meet and rotate in the direction opposite to the rotation of the crossed polarizers. This corresponds to a disclination with strength $-1/2$. Arrow c marks the position of dark grooves located between birefringent stripes. The birefringent stripes become dark when they are oriented along the polarizer or analyzer axes, but it is not possible to tell whether they are composed of clay particles oriented edge-to-edge, face-to-face, or for that matter face-to-edge. The black grooves do not seem to change in either brightness or position during rotation of the crossed polarizers. This is shown in Fig. 8, from which it seems reasonable that the black grooves correspond to regions of isotropic orientation, giving nematic-isotropic coexistence in almost every height of the settled suspension. Another possibility could be that there is homeotropic alignment in the black grooves and that the particles crosswise of the stripes orient in a helical structure similar to chiral (cholesteric) nematic phases. A way to test this could be to rotate the sample and see if the black grooves would move either up or down, since that would change the optical position of homeotropically aligned particles. However, this has not proved successful in our samples, since the increase in optical path length through our 1-mm-thick sample tubes changes the appearance of the pattern too much.

Defects in the nematic region close to the isotropic phase are shown in Fig. 9 for a gravity-settled sample of 3 wt% B3 powder at 1 mM NaCl. The pictures were taken after 8 months of settling. Arrow a shows a disclination of strength −1 and arrow b shows a disclination of strength +1. For all the samples that display Schlieren patterns, disclination points are found with both two (strength $-1/2$) and four (strength ± 1) emanating brushes. The disclinations seem to appear most frequently in the upper NS part, where larger domains are observed and the presence of (on average) smaller particles than in the lower phases was documented in [67].

V. CONCLUSIONS

We have studied stable strata of gravity-defined phase separation in suspensions of synthetic Na-fluorohectorite clay in saline solutions. We have observed and reported how the strata depend on clay concentration as well as on salt contents of the suspensions. The mass distribution in the isotropic and nematic phases, together with the density variation at the isotropic-nematic interface, indicates that existing models, and assumptions in existing simulations, may well account for the observed behavior, but that a precise determination of average particle diameters is needed to confirm this. We note that factors such as the high polydispersity and irregular shape of the present Na-fluorohectorite particles, as well as effects of the electrical double layers which could result in an overlap of, and even possibly a competition between nematic ordering and gelation in our system, may all contribute to determining the volume fraction at which the system transitions from an isotropic to an ordered state. It should also be noted that after a few weeks of gravitational settling, sedimentation due to gravity is more prominent in the isotropic sol than in the gelled nematic, thus leading to a lowering of the concentration of clay particles with time in the isotropic phase.

The dependence on ionic NaCl strength displays three main regimes irrespective of clay concentration. At low ionic strength ($\approx 0.1-5$ mM), the Debye screening length is presumably longer than the van der Waals force range. In this regime, the main mechanism for interparticle interaction should therefore be electrostatic repulsion and entropy-driven nematic ordering, in the Onsager sense, occurs. One may thus use the term "repulsive nematic" for this regime. For ionic strengths above about 5 mM, we believe that the van der Waals force come into play, meaning that gelation becomes important, and we may use the term "attractive nematic" for this regime. For ionic strengths above ≈ 10 mM, the clay particles form bigger assemblies due to the dominant van der Waals force and thus the nematic ordering is reduced.

We have studied the nematic phase in details between crossed polarizers and we have found textures showing nematic Schlieren patterns. By rotating polarizers as well as samples, we have seen examples of disclinations of strengths -1, $-1/2$, and $+1$.

In the majority of our images, a narrow nematic regime (NS) just at the interface of the isotropic-nematic transition is visible, with nematic ordering that differs from the larger NG phase. This is the subject of our recent study [67], along with ongoing studies on the dynamics of phase separation in gravity. We have previously shown that the nematic gel is sensitive to strong magnetic fields [44] and we plan to study this in more details in the future both in terms of nematic birefringent textures and also by means of x-ray scattering and MRI. We hope that our density measurements across the isotropic-nematic transition for the polydisperse NaFh system, and the comparison of these data to existing models and

simulations, could initiate theoretical or simulation work by other groups.

ACKNOWLEDGMENTS

We acknowledge the Research Council of Norway for funding through the FRINAT Project No. 171300/V30. We thank Ahmed Gmira for ion-exchanging parts of the NaFh powders used in the samples of the present paper and Zbigniew Rozynek for help with SEM imaging. We also wish to thank Kristina Kvashnina and the rest of the DUBBLE personnel for help during the ESRF experiments. We thank Mario Engelsberg for helpful discussions.

[1] J. C. P. Gabriel and P. Davidson, in *Colloid Chemistry 1*, edited by M. Antonietti (Springer, Berlin, 2003), Vol. 226, p. 119.
[2] P. Davidson and J. C. P. Gabriel, Curr. Opin. Colloid Interface Sci. **9**, 377 (2005).
[3] A. A. Sonin, T. Palermo, and A. Lubek, Mater. Chem. Phys. **56**, 74 (1998).
[4] H. Zocher, Z. Anorg. Allg. Chem. **147**, 91 (1925).
[5] F. C. Bawden, Nature (London) **138**, 1051 (1936).
[6] J. D. Bernal, J. Gen. Physiol. **25**, 111 (1941).
[7] Z. X. Zhang and J. S. van Duijneveldt, J. Chem. Phys. **124**, 154910 (2006).
[8] L. Onsager, Ann. N.Y. Acad. Sci. **51**, 627 (1949).
[9] R. Eppenga and D. Frenkel, Mol. Phys. **52**, 1303 (1984).
[10] J. A. C. Veerman and D. Frenkel, Phys. Rev. A **45**, 5632 (1992).
[11] I. Langmuir, J. Chem. Phys. **6**, 873 (1938).
[12] G. Broughton and L. Squires, J. Phys. Chem. **40**, 1041 (1936).
[13] E. A. Hauser, Chem. Rev. **37**, 287 (1945).
[14] E. A. Hauser and C. E. Reed, J. Phys. Chem. **41**, 911 (1937).
[15] K. Norrish, Discuss. Faraday Soc. **18**, 120 (1954).
[16] H. van Olphen, Discuss. Faraday Soc. **11**, 82 (1951).
[17] L. Bellon, M. Gibert, and R. Hernandez, Eur. Phys. J. B **55**, 101 (2007).
[18] I. Bihannic, L. J. Michot, B. S. Lartiges, D. Vantelon, J. Labille, F. Thomas, J. Susini, M. Salome, and B. Fayard, Langmuir **17**, 4144 (2001).
[19] D. Bonn, H. Kellay, H. Tanaka, G. Wegdam, and J. Meunier, Langmuir **15**, 7534 (1999).
[20] D. Bonn, J. Tanaka, G. Wegdam, H. Kellay, and J. Meunier, Europhys. Lett. **45**, 52 (1999).
[21] F. Cousin, V. Cabuil, and P. Levitz, Langmuir **18**, 1466 (2002).
[22] M. Dijkstra, J. P. Hansen, and P. A. Madden, Phys. Rev. Lett. **75**, 2236 (1995).
[23] A. Knaebel, M. Bellour, J. P. Munch, V. Viasnoff, F. Lequeux, and J. L. Harden, Europhys. Lett. **52**, 73 (2000).
[24] M. Kroon, G. H. Wegdam, and R. Sprik, Phys. Rev. E **54**, 6541 (1996).
[25] P. Levitz, E. Lecolier, A. Mourchid, A. Delville, and S. Lyonnard, Europhys. Lett. **49**, 672 (2000).
[26] C. Martin, F. Pignon, J. M. Piau, A. Magnin, P. Lindner, and B. Cabane, Phys. Rev. E **66**, 021401 (2002).
[27] L. J. Michot, I. Bihannic, K. Porsch, S. Maddi, C. Baravian, J. Mougel, and P. Levitz, Langmuir **20**, 10829 (2004).
[28] P. Mongondry, J. F. Tassin, and T. Nicolai, J. Colloid Interface Sci. **283**, 397 (2005).
[29] A. Mourchid, A. Delville, J. Lambard, E. Lecolier, and P. Levitz, Langmuir **11**, 1942 (1995).
[30] A. Mourchid, E. Lecolier, H. Van Damme, and P. Levitz, Langmuir **14**, 4718 (1998).
[31] F. Pignon, A. Magnin, and J. M. Piau, Phys. Rev. Lett. **79**, 4689 (1997).
[32] B. Ruzicka, L. Zulian, and G. Ruocco, Langmuir **22**, 1106 (2006).
[33] D. R. Strachan, G. C. Kalur, and S. R. Raghavan, Phys. Rev. E **73**, 041509 (2006).
[34] H. Tanaka, S. Jabbari-Farouji, J. Meunier, and D. Bonn, Phys. Rev. E **71**, 021402 (2005).
[35] H. Tanaka, J. Meunier, and D. Bonn, Phys. Rev. E **69**, 031404 (2004).
[36] J. C. P. Gabriel, C. Sanchez, and P. Davidson, J. Phys. Chem. **100**, 11139 (1996).
[37] C. Martin, F. Pignon, A. Magnin, M. Meireles, V. Lelievre, P. Lindner, and B. Cabane, Langmuir **22**, 4065 (2006).
[38] J. D. F. Ramsay and P. Lindner, J. Chem. Soc., Faraday Trans. **89**, 4207 (1993).
[39] J. D. F. Ramsay, S. W. Swanton, and J. Bunce, J. Chem. Soc., Faraday Trans. **86**, 3919 (1990).
[40] E. DiMasi, J. O. Fossum, T. Gog, and C. Venkataraman, Phys. Rev. E **64**, 061704 (2001).
[41] J. O. Fossum, E. Gudding, D. D. M. Fonseca, Y. Meheust, E. DiMasi, T. Gog, and C. Venkataraman, Energy **30**, 873 (2005).
[42] B. J. Lemaire, P. Panine, J. C. P. Gabriel, and P. Davidson, Europhys. Lett. **59**, 55 (2002).
[43] J. M. Saunders, J. W. Goodwin, R. M. Richardson, and B. Vincent, J. Phys. Chem. B **103**, 9211 (1999).
[44] E. N. de Azevedo, M. Engelsberg, J. O. Fossum, and R. E. de Souza, Langmuir **23**, 5100 (2007).
[45] P. Porion, M. Al Mukhtar, A. M. Faugere, R. J. M. Pellenq, S. Meyer, and A. Delville, J. Phys. Chem. B **107**, 4012 (2003).
[46] P. Porion, M. Al Mukhtar, S. Meyer, A. M. Faugere, J. R. C. van der Maarel, and A. Delville, J. Phys. Chem. B **105**, 10505 (2001).
[47] P. Porion, M. Al-Mukhtar, A. M. Faugere, and A. Delville, J. Phys. Chem. B **108**, 10825 (2004).
[48] P. Porion, A. M. Faugere, and A. Delville, J. Phys. Chem. B **109**, 20145 (2005).
[49] P. Porion, S. Rodts, M. Al-Mukhtar, A. M. Faugere, and A. Delville, Phys. Rev. Lett. **87**, 208302 (2001).
[50] S. Bhatia, J. Barker, and A. Mourchid, Langmuir **19**, 532 (2003).
[51] M. Kroon, W. L. Vos, and G. H. Wegdam, Phys. Rev. E **57**, 1962 (1998).
[52] J. Zhang, L. Y. Luan, W. X. Zhu, S. Y. Liu, and D. J. Sun, Langmuir **23**, 5331 (2007).
[53] M. C. D. Mourad, J. E. G. J. Wijnhoven, D. D. Van 't Zand, D. van der Beek, and H. N. W. Lekkerkerker, Philos. Trans. R. Soc. London, Ser. A **364**, 2807 (2006).

[54] D. van der Beek and H. N. W. Lekkerkerker, Europhys. Lett. **61**, 702 (2003).
[55] D. van der Beek and H. N. W. Lekkerkerker, Langmuir **20**, 8582 (2004).
[56] F. M. van der Kooij and H. N. W. Lekkerkerker, J. Phys. Chem. B **102**, 7829 (1998).
[57] L. J. Michot, I. Bihannic, S. Maddi, C. Baravian, P. Levitz, and P. Davidson, Langmuir **24**, 3127 (2008).
[58] L. J. Michot, I. Bihannic, S. Maddi, S. S. Funari, C. Baravian, P. Levitz, and P. Davidson, Proc. Natl. Acad. Sci. U.S.A. **103**, 16101 (2006).
[59] J. N. Israelachvili, *Intermolecular and Surface Forces* (Academic Press, London, 1991).
[60] V. A. Baulin, J. Chem. Phys. **119**, 2874 (2003).
[61] Z. Dogic, A. P. Philipse, S. Fraden, and J. K. G. Dhont, J. Chem. Phys. **113**, 8368 (2000).
[62] M. Schmidt, M. Dijkstra, and J. P. Hansen, J. Phys.: Condens. Matter **16**, S4185 (2004).
[63] A. E. Gonzalez, Phys. Rev. Lett. **86**, 1243 (2001).
[64] A. E. Gonzalez, G. Odriozola, and R. Leone, Eur. Phys. J. E **13**, 165 (2004).
[65] D. M. Fonseca, Y. Meheust, J. O. Fossum, K. D. Knudsen, K. J. Maloy, and K. P. S. Parmar, J. Appl. Crystallogr. **40**, s292 (2007).
[66] D. M. Fonseca, Y. Meheust, J. O. Fossum, K. D. Knudsen, and K. P. S. Parmar, Phys. Rev. E **79**, 021402 (2009).
[67] H. Hemmen, N. I. Ringdal, E. N. De Azevedo, M. Engelsberg, E. L. Hansen, Y. Méheust, J. O. Fossum, and K. D. Knudsen, Langmuir **25**, 12507 (2009).
[68] D. van der Beek, P. Davidson, H. H. Wensink, G. J. Vroege, and H. N. W. Lekkerkerker, Phys. Rev. E **77**, 031708 (2008).
[69] P. D. Kaviratna, T. J. Pinnavaia, and P. A. Schroeder, J. Phys. Chem. Solids **57**, 1897 (1996).
[70] K. D. Knudsen, J. O. Fossum, G. Helgesen, and V. Bergaplass, J. Appl. Crystallogr. **36**, 587 (2003).
[71] M. A. Bates and D. Frenkel, J. Chem. Phys. **110**, 6553 (1999).
[72] M. A. Bates, J. Chem. Phys. **111**, 1732 (1999).
[73] S. Abend and G. Lagaly, Appl. Clay Sci. **16**, 201 (2000).
[74] G. G. Peroli, G. Hillig, A. Saupe, and E. G. Virga, Phys. Rev. E **58**, 3259 (1998).